A Cultured Greigite-Producing Magnetotactic Bacterium in a Novel Group of Sulfate-Reducing Bacteria

Christopher T. Lefèvre, *et al.*

Science **334**, 1720 (2011);
DOI: 10.1126/science.1212596

A Cultured Greigite-Producing Magnetotactic Bacterium in a Novel Group of Sulfate-Reducing Bacteria

Christopher T. Lefèvre,[1,2,3] Nicolas Menguy,[4] Fernanda Abreu,[5] Ulysses Lins,[5] Mihály Pósfai,[6] Tanya Prozorov,[7] David Pignol,[1,2,3] Richard B. Frankel,[8] Dennis A. Bazylinski[9]*

Magnetotactic bacteria contain magnetosomes—intracellular, membrane-bounded, magnetic nanocrystals of magnetite (Fe_3O_4) or greigite (Fe_3S_4)—that cause the bacteria to swim along geomagnetic field lines. We isolated a greigite-producing magnetotactic bacterium from a brackish spring in Death Valley National Park, California, USA, strain BW-1, that is able to biomineralize greigite and magnetite depending on culture conditions. A phylogenetic comparison of BW-1 and similar uncultured greigite- and/or magnetite-producing magnetotactic bacteria from freshwater to hypersaline habitats shows that these organisms represent a previously unknown group of sulfate-reducing bacteria in the *Deltaproteobacteria*. Genomic analysis of BW-1 reveals the presence of two different magnetosome gene clusters, suggesting that one may be responsible for greigite biomineralization and the other for magnetite.

Several different groups of magnetotactic bacteria biomineralize magnetic mineral nanocrystals of magnetite (Fe_3O_4) and greigite (Fe_3S_4) through fundamentally different mechanisms (*1*). A number of magnetite-producing magnetotactic bacteria have been isolated and their genomes sequenced, revealing details about magnetite biomineralization at the molecular level (*2*–*4*), but no greigite-producing bacteria have been isolated and grown in axenic culture. There are two known morphological types of greigite-producers: a group of multicellular prokaryotes ["many-celled magnetotactic prokaryotes" (MMPs)], and a group of large rod-shaped bacteria (*5*). Although environmental studies revealed a good deal of information regarding MMPs (*6*–*11*), little is known about the large rod-shaped group except that some appear to produce magnetite as well as greigite in the same cell (*12*–*14*). One report describes a putative large, greigite-producing rod belonging to the *Gammaproteobacteria* (*8*), although its affiliation with this group is uncertain (*15*).

Here, we report a comprehensive phylogenetic analysis of large, rod-shaped, greigite- and/or magnetite-producing magnetotactic bacteria and the isolation and characterization of one of these microorganisms, strain BW-1, from a brackish spring at Badwater Basin, Death Valley National Park, California, USA. We collected water and sediment samples from numerous freshwater, brackish, and hypersaline aquatic environments located in the southwestern United States (table S1) (*16*). Although the magnetotactic bacterial populations in the samples were not homogeneous, the large rods were often the dominant magnetotactic bacterium present in the samples, as determined with microscopy by using the hanging drop technique (movie S1) (*17*). To obtain cells for analyses, magnetotactic bacteria were first magnetically enriched in sample bottles (*18*) and then purified using the magnetic racetrack procedure (*19*). After purification, cells were used to inoculate a variety of different growth media for electron microscopy, phylogenetic analysis, and fluorescence in situ hybridization.

We observed a wide range of large magnetotactic rods collected from different freshwater and saline environments (Fig. 1). In all cases, cells possessed a single polar flagellum (Fig. 1, A and D). Some cells contained mainly greigite (Fig. 1, A to C) or magnetite (Fig. 1, D to F), whereas others produced both minerals (Fig. 1, G to I, and table S1), as determined by means of selected-area electron diffraction (SAED) in the electron microscope. Although the morphologies of the greigite crystals were generally pleomorphic, in all cases the magnetite crystals were bullet- or arrowhead-shaped [elongated anisotropic (*20*)] (Fig. 1, E, F, H, and I). Using bacterial-specific primers for the 16*S* ribosomal RNA (rRNA)

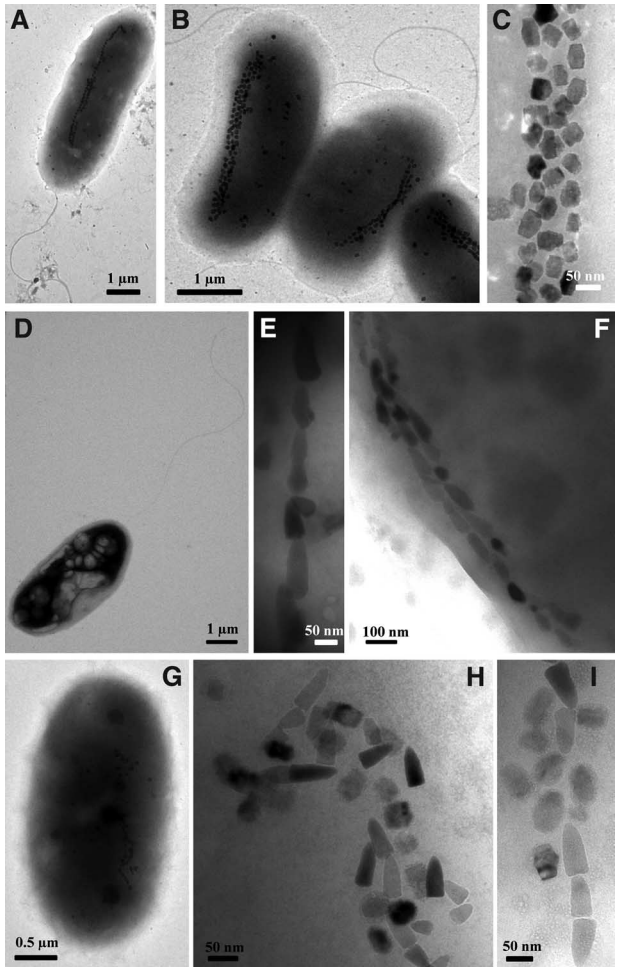

Fig. 1. Transmission electron microscope (TEM) images of uncultured, large, greigite- and/or magnetite-producing, rod-shaped bacteria. (**A** and **B**) TEM images of cells collected from a spring at ambient temperature in the Great Boiling Springs geothermal field in Gerlach, Nevada, USA. (**C**) High-magnification TEM image of greigite crystals from the cell shown in (B). (**D**) TEM image of a cell collected from Lake Mead, Nevada, USA. (**E**) High-magnification TEM image of magnetosomes in cell shown in (D). Magnetosome crystals in this cell are bullet-shaped magnetite. (**F**) TEM image of cell collected from Bridgeport Reservoir, Bridgeport, California, USA, showing double chain of bullet-shaped magnetite crystals. (**G**) TEM image of a cell collected from a freshwater pond close to Zion National Park, Utah, USA. (**H** and **I**) High-magnification TEM images of magnetosomes in (G) showing greigite and bullet-shaped magnetite crystals aligned in the same chains.

[1]Laboratoire de Bioénergétique Cellulaire, UMR 6191, Commissariat à l'Énergie Atomique Cadarache, Direction des Sciences du Vivant, Institut de Biologie Environnementale et Biotechnologie, Saint-Paul-lez-Durance 13108, France. [2]Biologie Végétale et Microbiologie Environnementale, UMR 6191, CNRS, Saint-Paul-lez-Durance 13108, France. [3]Université Aix-Marseille, Saint-Paul-lez-Durance, 13108, France. [4]Institut de Minéralogie et de Physique des Milieux Condensés Université Pierre et Marie Curie UMR CNRS 7590–Institut de Recherche pour le Développement 4, place Jussieu, 75005 Paris, France. [5]Instituto de Microbiologia Professor Paulo de Góes, Universidade Federal do Rio de Janeiro, 21941-590 Rio de Janeiro, RJ, Brazil. [6]Department of Earth and Environmental Sciences, University of Pannonia, Veszprém H8200, Hungary. [7]Ames Laboratory, U.S. Department of Energy, Ames, IA 50011, USA. [8]Department of Physics, California Polytechnic State University, San Luis Obispo, CA 93407, USA. [9]University of Nevada at Las Vegas, School of Life Sciences, Las Vegas, Nevada 89154–4004, USA.

*To whom correspondence should be addressed. E-mail: dennis.bazylinski@unlv.edu

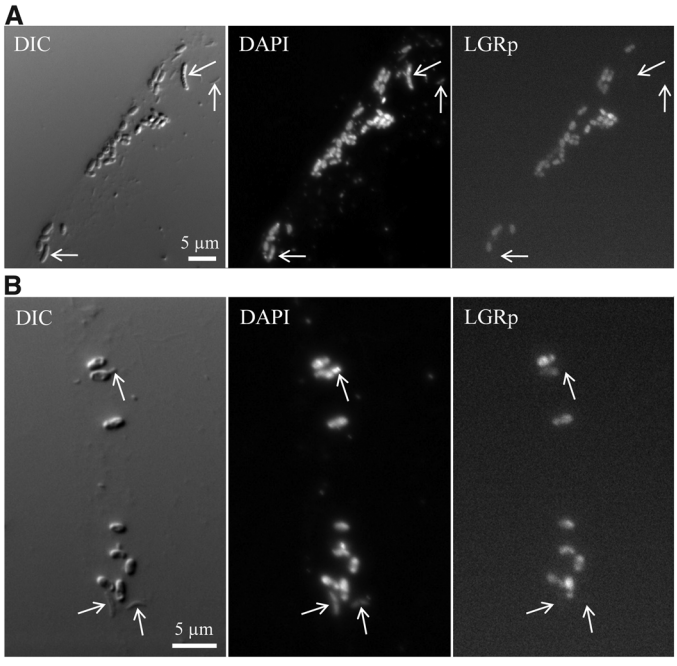

Fig. 2. Fluorescent in situ hybridization (FISH) of large, greigite- and/or magnetite-producing, rod-shaped magnetotactic bacteria (LGRs) to the specific oligonucleotide rRNA probe (LGRp). (**A**) FISH of LGR cells collected from Badwater Basin, Death Valley National Park, California, USA. (**B**) FISH of LGR cells collected from Rogers Spring at the Lake Mead National Recreation Area, Nevada, USA. (Left) Differential interference contrast (DIC) images of magnetically enriched cells from water and sediment samples. (Middle) fluorescence microscope images of the same cells stained with 4′,6-diamidino-2-phenylindole (DAPI). (Right) fluorescence microscope images of the same cells hybridized with the LGR-specific Alexa594-labeled probe LGRp (5′-GCTGCCCTCTGTACATAC-3′, complementary to nucleotides close to the 1260–base pair region of the 16*S* rRNA molecule of the different LGRs). Cells at arrows are not LGRs and serve here as negative controls because only LGRs cells fluoresced with this probe.

gene and polymerase chain reaction (*21*), we obtained 25 nearly complete 16*S* rRNA gene sequences from these rod-shaped organisms collected from 12 different sites. Using specific oligonucleotide probes designed from these sequences and in situ fluorescent hybridization, we authenticated the 16*S* rRNA gene sequences obtained from these organisms (Fig. 2).

Phylogenetic analysis of the 16*S* rRNA gene sequences from the large rod-shaped magnetotactic bacteria show that these organisms form a clade within the sulfate-reducing bacteria in the *Deltaproteobacteria* class of the *Proteobacteria* phylum that does not contain any other known cultured bacteria (Fig. 3). This clade appears to consist of at least two smaller groups, each constituting at least two genera based on 16*S* rRNA divergence. We were unable to correlate the separation of these subgroups with cell morphology, environmental parameters of the organisms' habitat such as salinity, or composition of magnetosome crystals.

Our phylogenetic results appear to contradict the recent assignment of an uncultured, putative, greigite-producing rod to the *Gammaproteobacteria* (*8*); however, the group-specific 23*S* RNA-targeted probe GAM42a for this bacterium (*22*) does not allow for the unambiguous binding of any gammaproteobacterial-specific sequences

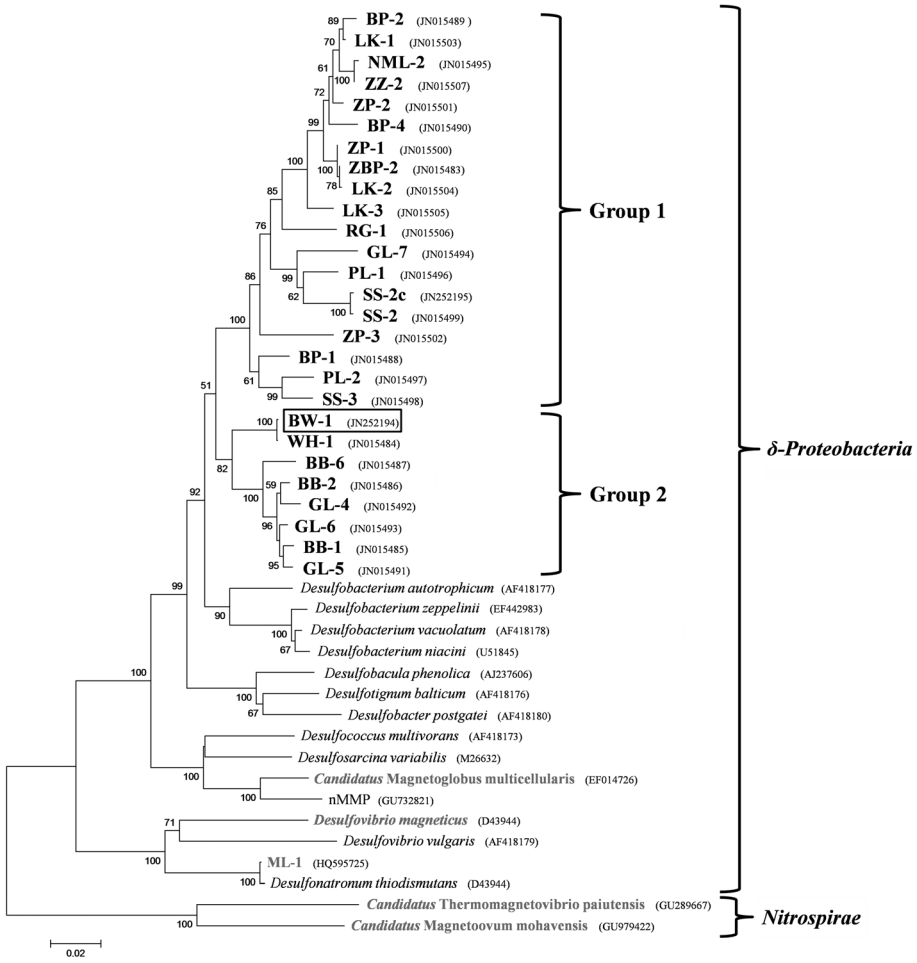

Fig. 3. Phylogenetic tree, based on 16*S* rRNA gene sequences, showing the phylogenetic position of LGRs in the *Deltaproteobacteria* class. Bootstrap values at nodes are percentages of 1000 replicates. 16*S* rRNA gene sequences of the uncultured magnetotactic bacteria *Candidatus* Thermomagnetovibrio paiutensis (*28*) and *Ca.* Magnetoovum mohavensis (*29*) of the *Nitrospirae* phylum were used to root the tree. GenBank accession nos. are given in parentheses. Bar represents 2% sequence divergence. Letters in sequence designations indicate sampling site listed in table S1, and numbers following represent clone number. BP, Bridgeport Reservoir; LK, Lake Mead; NML, freshwater pond near Mono Lake; ZZ, Lake Tuendae; ZP, freshwater pond near Zion National Park; ZBP, Zuma Beach; RG, Rogers Spring; GL, pools at Great Boiling Springs; PL, Pyramid Lake; SS, Salton Sea; SS-2c, lagoon at Salton Sea; BB, Badwater Basin; and WH, Salt Pond. Details and exact coordinates are provided in table S1. BW-1 refers to the cultured LGR described in the text.

to this bacterium (*15*). The recent discovery of magnetite-producing rods that belong to the *Gammaproteobacteria* and are found in the same habitats as rod-shaped greigite-producers (*18*) might also explain this discrepancy.

Magnetically purified, large, rod-shaped, magnetotactic bacteria from several sites were inoculated into a variety of growth media. Growth of some of these organisms was observed in an anaerobic, complex, liquid growth medium for the enrichment of heterotrophic sulfate-reducing bacteria. Through three successive rounds of dilution to extinction in this medium, two pure cultures were obtained: strain BW-1 from Badwater Basin and strain SS-2 from the Salton Sea (California, USA). Both strains phylogenetically lie within the clade of the uncultured large rods in the *Deltaproteobacteria* class (Fig. 3). Strain SS-2 appeared to only biomineralize magnetite under our culture conditions.

In culture, BW-1 produces one or two loose chains of magnetosomes that contain greigite and/or magnetite, as determined through a combination of elemental mapping by using energy-filtered imaging (figs. S1 and S2) and electron diffraction (Fig. 4, A to C, and figs. S2C and S3B). Magnetosome mineral composition correlated with the concentration of hydrogen sulfide formed during growth. For example, when sulfide was allowed to accumulate in the growth medium (>0.3 mM sulfide) most magnetosomes contained greigite (Fig. 4, and figs. S1 and S2). When the headspace of the cultures was purged every other day with oxygen-free argon gas so as to decrease the concentration of hydrogen sulfide in the cultures (<0.3 mM), cells contained chains of bullet-shaped, magnetite-containing magnetosomes (fig. S3). Thus, whether greigite and/or magnetite are produced in the magnetosomes of these organisms is affected by external environmental conditions such as hydrogen sulfide concentration and/or redox potential. This finding is consistent with observations on uncultured rod-shaped, greigite-producing magnetotactic bacteria in a chemically stratified, oxygen/sulfide inverse gradient system (*13*).

Magnetite crystals produced by BW-1 were consistently bullet-shaped, whereas greigite crystals had irregular outlines and lacked a well-defined crystal habit (Fig. 4, B and C). Thin sections of greigite magnetosomes reveal an electron-dense layer surrounding the crystal that is consistent with the presence of a magnetosome membrane (Fig. 4, E and F), which has also been observed in greigite magnetosomes of the MMP *Candidatus* Magnetoglobus multicellularis (*23*).

Our sampling effort demonstrates that greigite-producing magnetotactic bacteria are not confined to marine habitats as previously thought (*8*). Although several of these organisms collected from different sites appeared to only contain magnetite, it seems likely that all can biomineralize greigite under the appropriate conditions (such as when sulfate is present as the terminal electron acceptor and is reduced to sulfide), on the basis of evidence presented here and on the fact that environmental conditions are thought to have an effect on the magnetosome mineral produced in these organisms (*13*). Although they differ morphologically, there are several similarities between the large rods and the greigite-producing MMP group. These obligately multicellular organisms consist of 10 to 60 genetically identical cells and are also phylogenetically affiliated with the *Deltaproteobacteria* class of the *Proteobacteria* phylum (*9*–*11*, *24*). Some are known to biomineralize magnetite as well as greigite (*25*), and based on phylogenetic and genetic evidence, the MMPs appear to be anaerobic, sulfate-reducing bacteria (*9*–*11*, *24*).

Recently, magnetosome (*mam*) genes, similar to those in magnetite-producing magnetotactic bacteria, have been found in an MMP that produced only greigite, leading to the idea that the magnetotactic trait, whether based on iron oxide or iron sulfide production, is monophyletic (*26*). The fact that magnetite and/or greigite production can be controlled in cells of a single species by modifying the external chemistry and redox potential suggests that there might be specific genes involved in greigite production in some large rods and MMPs that are expressed in certain conditions. We identified *mam* genes in the genome of strain BW-1 that are mostly present as two copies (table S2) and appear to form two separate clusters (fig. S5). The first cluster contains genes encoding for magnetosome proteins most closely related to those of the magnetite-producer *Desulfovibrio magneticus* strain RS-1 (*27*). The second cluster contains genes encoding for proteins most closely related to those of the greigite-producer *Candidatus* Magnetoglobus multicellularis (*26*). These results point to the possibility that different forms of *mam* genes are responsible for magnetite (cluster one) and greigite (cluster two) biomineralization (fig. S5) and that the two gene clusters are regulated differentially, resulting in different proportions of magnetite and greigite in cells.

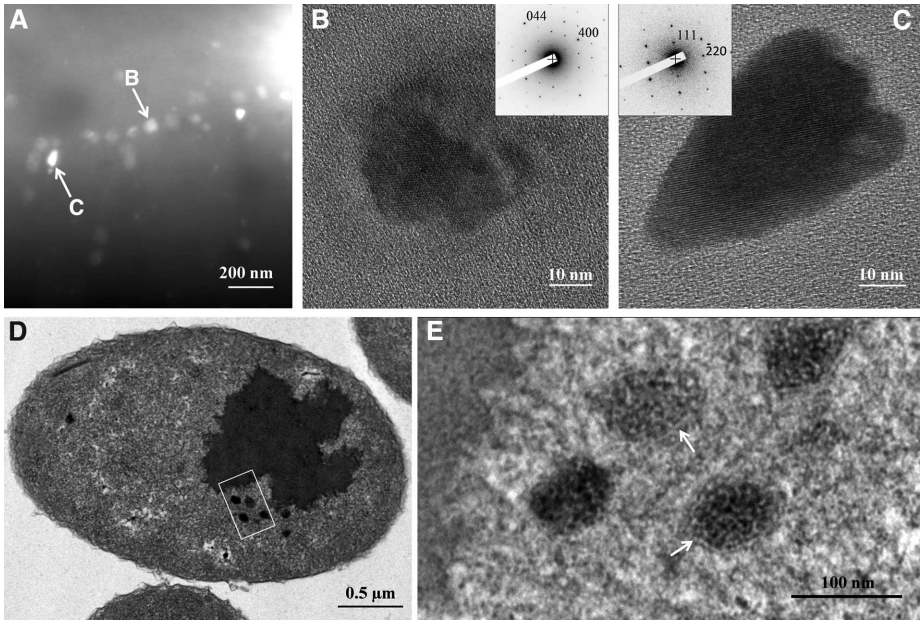

Fig. 4. TEM images of strain BW-1. (**A**) Darkfield scanning TEM image of a magnetosome chain containing both greigite (labeled B) and magnetite (labeled C). (**B**) High-magnification TEM image of greigite crystal labeled in (A). (Inset) SAED of crystal viewed along the [0 −1 1] zone axis. Pattern is consistent with greigite. (**C**) High-magnification TEM image of magnetite crystal labeled in (A). (Inset) SAED pattern of crystal viewed along the [−1 −1 2] zone axis. (**D**) TEM image of a stained thin-section of a cell of BW-1 showing several magnetosomes aligned in the cell. Dark, intracellular, electron-dense mass represents large cell inclusion that is also visible by use of light microscopy. (**E**) High-magnification TEM image of magnetosomes in (D) showing that an electron-dense layer surrounds the greigite crystals, suggesting the presence of a magnetosome membrane.

References and Notes

1. R. B. Frankel, D. A. Bazylinski, *Rev. Mineral.* **54**, 95 (2003).
2. D. A. Bazylinski, R. B. Frankel, *Nat. Rev. Microbiol.* **2**, 217 (2004).
3. A. Komeili, *Annu. Rev. Biochem.* **76**, 351 (2007).
4. D. Schüler, *FEMS Microbiol. Rev.* **32**, 654 (2008).
5. S. Spring, D. A. Bazylinski, *Prokaryotes* **2**, 842 (2006).
6. S. Mann, N. H. C. Sparks, R. B. Frankel, D. A. Bazylinski, H. W. Jannasch, *Nature* **343**, 258 (1990).
7. M. Farina, D. Motta de Esquivel, H. G. P. Lins de Barros, *Nature* **343**, 256 (1990).
8. S. L. Simmons, S. M. Sievert, R. B. Frankel, D. A. Bazylinski, K. J. Edwards, *Appl. Environ. Microbiol.* **70**, 6230 (2004).
9. F. Abreu *et al.*, *Int. J. Syst. Evol. Microbiol.* **57**, 1318 (2007).
10. S. L. Simmons, K. J. Edwards, *Environ. Microbiol.* **9**, 206 (2007).
11. R. Wenter, G. Wanner, D. Schüler, J. Overmann, *Environ. Microbiol.* **11**, 1493 (2009).
12. D. A. Bazylinski, B. R. Heywood, S. Mann, R. B. Frankel, *Nature* **366**, 218 (1993).
13. D. A. Bazylinski *et al.*, *Appl. Environ. Microbiol.* **61**, 3232 (1995).
14. T. Kasama *et al.*, *Am. Mineral.* **91**, 1216 (2006).

15. R. Amann, J. Peplies, D. Schüler, in *Magnetoreception and Magnetosomes in Bacteria*, D. Schüler, Ed. (Springer-Verlag, Berlin Heidelberg, 2007), pp. 25–36.
16. Materials and methods are available as supporting material on *Science* Online.
17. D. Schüler, *Int. Microbiol.* **5**, 209 (2002).
18. C. T. Lefèvre *et al*., *ISME J.*, published online 21 July 2011 (10.1038/ismej.2011.97).
19. R. S. Wolfe, R. K. Thauer, N. Pfennig, *FEMS Microbiol. Lett.* **45**, 31 (1987).
20. C. T. Lefèvre *et al*., *Earth Planet. Sci. Lett.* **312**, 194 (2011).
21. D. J. Lane, in *Nucleic Acid Techniques in Bacterial Systematics*, E. Stackebrandt, M. Goodfellow, Eds. (Wiley, Chichester, 1991), pp. 115–175.
22. W. Manz, R. Amann, W. Ludwig, M. Wagner, K.-H. Schleifer, *Syst. Appl. Microbiol.* **15**, 593 (1992).
23. F. P. Abreu, K. T. Silva, M. Farina, C. N. Keim, U. Lins, *Int. Microbiol.* **11**, 75 (2008).
24. E. F. DeLong, R. B. Frankel, D. A. Bazylinski, *Science* **259**, 803 (1993).
25. U. Lins, C. N. Keim, F. F. Evans, P. R. Buseck, M. Farina, *Geomicrobiol. J.* **24**, 43 (2007).
26. F. Abreu *et al*., *ISME J.* **5**, 1634 (2011).
27. H. Nakazawa *et al*., *Genome Res.* **19**, 1801 (2009).
28. C. T. Lefèvre *et al*., *Appl. Environ. Microbiol.* **76**, 3740 (2010).
29. C. T. Lefèvre, R. B. Frankel, F. Abreu, U. Lins, D. A. Bazylinski, *Environ. Microbiol.* **13**, 538 (2011).

Acknowledgments: This work was partially supported by U.S. National Science Foundation grant EAR-0920718 (D.A.B.) and by a grant from the Fondation pour la Recherche Médicale SPF20101220993 (C.T.L.). Part of the transmission electron microscopy characterization was carried out in Ames Lab and was supported by the U.S. Department of Energy, Basic Energy Sciences, Materials Sciences and Engineering Division. The Ames Laboratory is operated for the U.S. Department of Energy by Iowa State University under contract DE-AC02-07CH11358. We thank F. Mahlaoui and M. L. Schmidt for help with sampling; the National Park Service staff of Death Valley National Park; and the team at the Laboratório de Bioinformática, Laboratório Nacional de Computação Científica, Rio de Janeiro, Brazil, for their help in the sequencing and annotation of the genome of strain BW-1. Samples at Death Valley National Park were collected under Sampling Permit DEVA-2010-SCI-0038 issued by the U.S. Department of the Interior National Park Service. 16*S* rRNA gene sequences (accession nos. JN015483 to JN015507, JN252194, and JN25219), gene for adenosine-5′-phosphate reductase (*aprA*; JN705544) and *mam* genes of BW-1 (JN830627 to JN830646 and JN845570 to JN845575) are published in GenBank. Strain BW-1 has been deposited to the Japan Collection of Microorganisms, RIKEN BioResource Center under the provisional name *Candidatus* Desulfamplus magnetomortis and carries accession no. JCM 18010.

Supporting Online Material

www.sciencemag.org/cgi/content/full/334/6063/1720/DC1
Materials and Methods
SOM Text
Figs. S1 to S6
Tables S1 and S2
References (*30*–*39*)
Movies S1 and S2

12 August 2011; accepted 2 November 2011
10.1126/science.1212596

The Ribosome Modulates Nascent Protein Folding

Christian M. Kaiser,[1,2] Daniel H. Goldman,[3] John D. Chodera,[1] Ignacio Tinoco Jr.,[1,3] Carlos Bustamante[1,2,3,4,5]*

Proteins are synthesized by the ribosome and generally must fold to become functionally active. Although it is commonly assumed that the ribosome affects the folding process, this idea has been extremely difficult to demonstrate. We have developed an experimental system to investigate the folding of single ribosome-bound stalled nascent polypeptides with optical tweezers. In T4 lysozyme, synthesized in a reconstituted in vitro translation system, the ribosome slows the formation of stable tertiary interactions and the attainment of the native state relative to the free protein. Incomplete T4 lysozyme polypeptides misfold and aggregate when free in solution, but they remain folding-competent near the ribosomal surface. Altogether, our results suggest that the ribosome not only decodes the genetic information and synthesizes polypeptides, but also promotes efficient de novo attainment of the native state.

Proteins can spontaneously fold into their native structures under appropriate conditions (*1*). In vitro, some small proteins and single domains attain their native structures within microseconds (*2*), whereas topologically complex and larger proteins may require many seconds to fold (*3*) and often populate folding intermediates along the way (*4*, *5*). In vivo, however, folding is not necessarily limited to full-length proteins or domains. Proteins can begin to fold before they are fully synthesized and while still bound to the ribosome (*6*–*12*). Moreover, during protein synthesis on the ribosome (*13*), elongation rates are regulated by factors including tRNA abundance (*14*), codon order (*15*), and mRNA secondary structure (*16*). Decreasing these rates locally (*17*, *18*) or globally (*19*) can affect the folding efficiency of newly synthesized proteins. The complete synthesis of even small proteins (100 amino acids or less) requires at least several seconds at a maximum rate of ~20 amino acids per second in *Escherichia coli* (*20*), giving nascent-chain segments sufficient time to conformationally equilibrate in the environment of the ribosome, perhaps adopting structures that are distinctly different from the native protein fold (*7*, *21*). However, the observation of folding transitions in ribosome-bound nascent proteins has not been possible, and a detailed analysis has been limited to computational approaches (*22*, *23*).

We have developed an experimental system to directly probe the folding of single ribosome-bound nascent chains (*24*, *25*) by subjecting them to force using optical tweezers (Fig. 1 and figs. S1 to S3). The force is applied between the nascent chain and the large ribosomal subunit. Because force acts locally (*26*, *27*), we can selectively perturb the stability of ribosome-bound nascent polypeptides without disrupting the structural integrity of the ribosome. We studied a cysteine-free version of T4 lysozyme (*28*), a monomeric cytosolic protein composed of two globular regions, or subdomains (Fig. 1, C and D). T4 lysozyme folding has been studied in ensemble (*29*–*31*) and single-molecule (*27*) experiments. The native fold requires interactions between the N- and C-terminal sequences whose synthesis is separated in time during vectorial translation by the ribosome.

Using a reconstituted in vitro translation system supplemented with *E. coli* ribosomes (*32*), we first translated the protein with an unstructured C-terminal extension of 41 amino acids such that the entire T4 lysozyme sequence emerges from the narrow ribosomal exit tunnel (*33*). This experimental design allows us to study the folding dynamics of the full-length protein on the ribosome. When we stretched the molecule by continuously increasing the tension applied across the nascent chain ("force ramp"), we observed single rips in the resulting force-extension traces, representing cooperative unfolding events (Fig. 1E). Puromycin-release experiments confirmed that these signals originated from ribosome-bound nascent proteins (fig. S4).

The mechanical unfolding pathways of free and ribosome-bound full-length T4 lysozyme are very similar: The latter unfolds at a mean force (F_{Unf}) of 17.0 ± 2.0 pN (N = 125 unfolding events) at a pulling speed of 100 nm/s (Fig. 1G). Using the wormlike chain (WLC) model (*34*), we calculated a contour length increase upon unfolding (ΔL_C) of 59.9 ± 2.1 nm, consistent with the value expected for full-length T4 lysozyme (164 amino acids × 0.36 nm per amino acid – 0.9 nm corresponding to the folded end-to-end distance = 58.1 nm). Experiments with the free protein in the absence of the ribosome (Fig. 1, F and H) revealed similar unfolding characteristics (F_{Unf} = 17.2 ± 1.8 pN, ΔL_C = 60.1 ± 0.9 nm, N = 453), confirming that the entire protein is able to emerge from the ribosomal tunnel by means of the 41–amino acid linker (*33*). Analysis of the unfolding force distributions (*35*) of free and ribosome-bound polypeptides (Fig. 1, G and H) also reveals similar distances to the transition state ($\Delta^{\ddagger}x_{\mathrm{free}}$ = 2.3 ± 0.5 nm, $\Delta x^{\ddagger}_{\mathrm{ribosome\text{-}bound}}$ = 2.0 ±

[1]Institute for Quantitative Biosciences (QB3), University of California, Berkeley, CA 94720, USA. [2]Department of Physics, University of California, Berkeley, CA 94720, USA. [3]Department of Chemistry, University of California, Berkeley, CA 94720, USA. [4]Department of Molecular and Cell Biology, University of California, Berkeley, CA 94720, USA. [5]Howard Hughes Medical Institute, University of California, Berkeley, CA 94720, USA.

*To whom correspondence should be addressed. E-mail: carlos@alice.berkeley.edu